

GT2011-458- (

COAL ASH DEPOSITION ON NOZZLE GUIDE VANES: PART I - EXPERIMENTAL CHARACTERISTICS OF FOUR COAL ASH TYPES

J. Webb, B. Casaday, B. Barker, J. P. Bons
Department of Mechanical and Aerospace Engineering
Ohio State University
Columbus, OH 43235
and

A.D. Gledhill, N.P. Padture
Department of Materials Science Engineering
Ohio State University
Columbus, OH 43235

ABSTRACT

An accelerated deposition test facility was operated with three different coal ash species to study the effect of ash composition on deposition rate and spatial distribution. The facility seeds a combustor (natural gas) flow with 10-20 micron mass mean diameter coal ash particulate. The particulate-laden combustor exhaust is accelerated through a rectangular-to-annular transition duct and expands to ambient pressure through a nozzle guide vane annular sector. For the present study, the annular cascade consisted of two CFM56 aero-engine vane doublets; comprising three full passages and two half passages of flow. The inlet Mach number (0.1) and gas temperature (1100°C) are representative of operating turbines. Ash samples were tested from the three major coal ranks: lignite, subbituminous, and bituminous. Investigations over a range of inlet gas temperatures from 900°C to 1120°C showed that deposition increased with temperature, though the threshold for deposition varied with ash type. Deposition levels varied with coal rank, with lignite producing the largest deposits at the lowest temperature. Regions of heightened deposition were noted; the leading edge and pressure surface being particularly implicated. Scanning electron microscopy was used to identify deposit structure. For a limited subset of tests, film cooling was employed at nominal design operating conditions but provided minimal protection in cases of severe deposition.

INTRODUCTION

The push to become a more environmentally conscious society has grown significantly in recent years and large strides have recently been made in power generation. Modern coal gasification power facilities have greatly improved the efficiency in creating electricity for the masses. Unfortunately, the coal gasification process produces a fuel with fly ash particulate that may enter the gas turbine combustor and pass through the hot sections of the turbine, depositing on turbine components. These syn-fuels can be cleaned, but small amounts of particulate will still be ingested

[1]. This has caused a resurgence of deposition study in an attempt to understand the effects of the deposits and attempts at mitigating deposit formation. Particulate can also be ingested at the engine's air intake. This can come from aero engines flying through volcanic clouds, or in the case of power generation turbines from dust that has mixed with ambient air. Most modern power generation gas turbine filtration techniques only remove particles greater than 10 μm which is not adequate enough to entirely stop deposit formation.

The effects of deposition are well documented in the literature. Kim et. al. [2] investigated deposition on modern turbine combustors and high pressure turbine vanes with the ingestion of volcanic ash. It was found that the rate at which deposition occurs increases with time for a given dust concentration and inlet temperature. Damage to Nozzle Guide Vanes (NGV's) can occur if deposits block the leading edge film cooling holes causing the blades to burn out. Figure 1 illustrates the damage that deposition can inflict upon high pressure turbine rotors. Dunn et al. [3] investigated deposition by exposing modern aero engines to a volcanic ash cloud. They found that deposition on the NGV's increased the combustor static pressure and that turbine inlet temperatures on the order of 1093°C are high enough to allow deposition. Wenglarz showed that when the throat area in nozzle guide vanes (NGV's) is decreased by deposition the overall power generated by the turbine is reduced [4]. Deposition also severely increases the roughness on the vane surface. Bogard et al found that surface roughness can increase heat transfer by 50% over a smooth surface [5].

Numerical studies have also shed significant light on the mechanics of deposition in turbomachines. Some of the first studies of particle impacts in turbines were done by Hussein and Tabakoff [6]. Their studies indicated a significant increase in particle impacts with increases in particle size (i.e. Stokes number) and particle velocity. Later studies by the same group experimentally validated these trajectories [7]. Models have since been developed that predict particle sticking based on the velocity and/or chemical composition of the ash. For example, Tafti and Sreedharan [8] developed a model that

predicted deposition on a wedge shaped geometry and compared them to experiment. They noted that most deposition takes place near the stagnation region with the capture efficiency increasing exponentially with temperature. A more in depth review of computational studies may be found in the Part II companion paper [9].

It is clear that understanding turbine deposition is important but large-scale tests such as those mentioned above are costly and time consuming. Simulated particle deposition experiments are an attractive, economical alternative to full engine testing. For example, Lawson and Thole [10] used a flat plate with film cooling holes and a low melting temperature wax to investigate reduced film cooling effectiveness with surface deposition. It was found that deposition in and around film cooling holes reduced cooling effectiveness by approximately 20% at moderate momentum flux ratios. Vandsburger et al. [11] also studied deposition of simulated ash particles on leading edge film cooling holes and found that particle capture efficiency increased substantially with temperature. They used Teflon and PVC particles to simulate fly ash so lower operating temperatures could be used. Both Vandsburger and Lawson used Stokes number to correlate the simulated particles to coal ash.

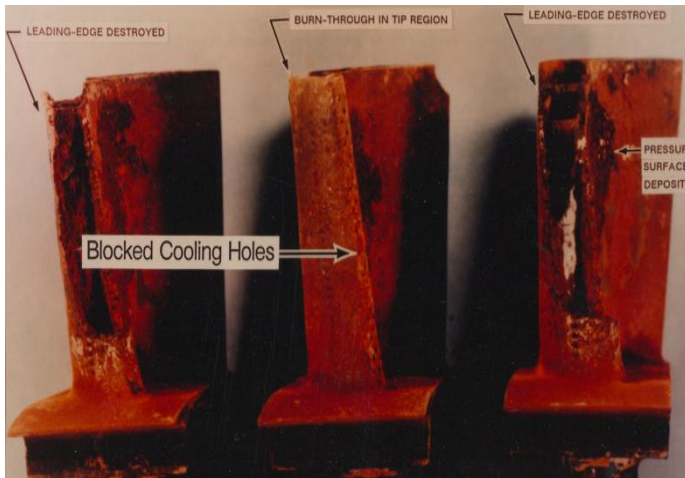


Figure 1: Volcanic Ash Deposition Damage to High Pressure Turbine Rotor (from Kim et al. [2])

These simulated ash studies do well to model some aspects of deposit growth but the need exists for facilities that generate actual ash deposits with temperatures and velocities that compare closely to in service power generation turbines. Jensen et. al [12] describe the construction and validation of a facility that exposes one inch diameter coupons to flow with turbine inlet conditions and seeded with coal fly ash. This facility was then used by Crosby et al. [13] who characterized the effects of particle size and temperature on deposition, finding the onset of deposition to begin at 960°C and noting that deposition increases with particle size. Smith et al [14] present a facility that exposes real turbine hardware to an environment analogous to that experienced at the exit of a combustor and is able to illustrate the effect of film cooling rates and temperature on deposit formation. It was found that

both inlet temperature and film cooling play a significant role in the deposition process.

The present study further validates the facility described in Smith et al. [14] by using four different coal fly ash samples to create deposition on actual turbine hardware and comparing the deposits to those created on in-service hardware.

EXPERIMENTAL FACILITY

A thorough description of the Turbine Reacting Flow Rig (TuRFR) pictured in Figure 2 can be found in Smith et. al. [14]; for the current paper only a brief summary is provided. High pressure air passes through a regulator and 2 choked flow orifice flowmeters. The flow is then divided into the necessary flow paths to provide the main airflow, film cooling, pre-mixing and particulate flow. The main air is introduced into the base of the rig via 4 equally spaced pipes feeding into a rock bed and honeycomb to disperse and straighten the flow before it enters the combustion zone.

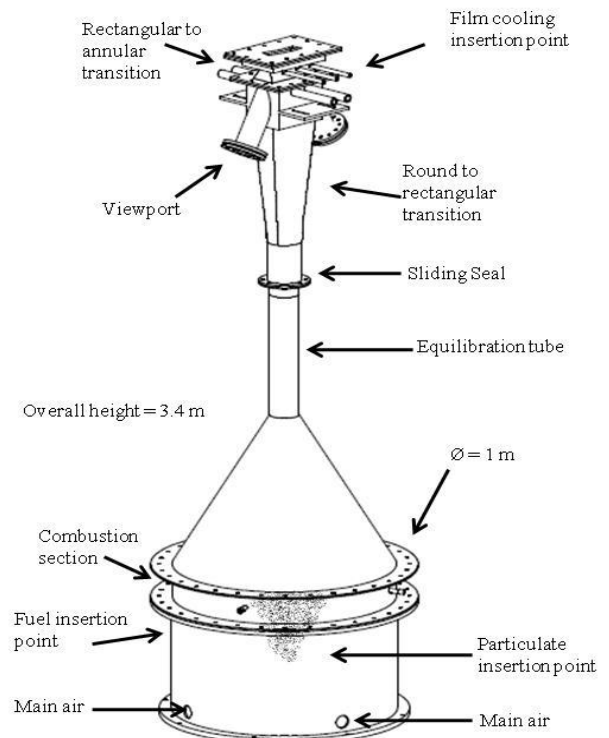


Figure 2: Schematic of TuRFR showing primary flow path, particulate, fuel and film cooling insertion points

In the combustion zone the air is heated to temperatures comparable to modern gas turbines by the burning of natural gas. Thirty-two flame holders are spaced within the combustion zone to facilitate mixing of the combustion products and decrease sooting. At this point the air is also seeded with particulate via an insertion tube in the center of the rig. After the combustion zone the air is accelerated through an axisymmetric cone with an inlet to exit area ratio of 68:1 producing Mach numbers between 0.07 to 0.1 depending on the temperature and mass flow rate. The flow then proceeds through an equilibration tube that allows the particles to come to a thermal and kinetic balance with the airflow. The flow then enters a transition section which includes the measurement and viewing areas. A cutaway of this measurement and

viewing area is shown in Figure 3 with the optical path and measurement locations marked. As described in Smith et. al [14] this section also includes 2 removable plates separating 2 cavities from the main airflow that are used to replicate temperature gradients produced by dilution jets. These cavities were not utilized for the current study.

Lastly, flow enters a rectangular to annular transition where 2 NGV doublets are held. For the current study, NGV's from a CFM56-5B aero engine were utilized, but for future work this upper transition may be modified to encompass any number of blade designs. The vanes are not coated with thermal barrier or anti-oxidation coatings. The two doublets encompass 4 vanes, producing 3 full passages and 2 half passages of flow with an inlet area of approximately 0.0132 m^2 . The NGV's then exhaust directly to atmosphere.

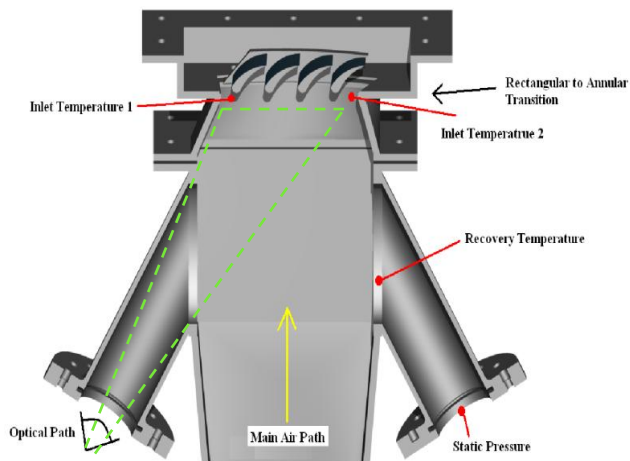


Figure 3: Cutaway of TuRFR showing optical access

As mentioned above, air is diverted from the main flow to provide for auxiliary facility systems such as film cooling and particulate insertion. The film cooling cavities are located on both the hub and casing sides of the vanes; air enters the hollow vanes via these cooling cavities. Film cooling density ratio is calculated by measuring the temperature ratio between the NGV inlet plane and the film cooling cavities. Mass flow rates for both the hub and casing film cooling cavities are measured using two inline pneumatic flow meters.

Auxiliary air is also used to supply the particle feed system. The flow travels through a venturi tube to reduce static pressure; this static pressure reduction is used to pull particles from the pressurized particulate feeder into the flow path. The particulate feeder consists of an auger/agitator configuration which pulls the particulate down from a pressurized hopper. The auger/agitator is connected to a DC motor and by controlling the speed at which the auger rotates; the particulate feed rate can be proscribed.

COAL ASH PROPERTIES

Four different coal ash samples were investigated spanning the full spectrum of coal ranks available to power generation facilities. One ash derived from bituminous coal mined from West Virginia, a lignite ash from Mississippi, and two sub-bituminous ash samples from coal mined in two

different parts of Wyoming. One sub-bituminous ash was derived from coal mined in the Powder River Basin (PRB) in northeastern Wyoming and the other derived from coal mined at the Jim Bridger Power Station (JBPS) in southwestern Wyoming. All samples are from the hot gas filter hopper of operating power plants.

The composition of the four ashes was analyzed with wavelength dispersive X-ray fluorescence (WD-XRF). The ash was diluted in a 10:1 ratio in a lithium borate flux. The flux used was a 1:2 mixture by weight of lithium tetraborate to lithium metaborate with an added 1% by weight of lithium iodine as a non-wetting agent. The ash was dissolved in the flux, homogenized, and cast into 40mm discs in an automatic bead-making furnace. The fused beads were then analyzed in the WD-XRF with a rhodium X-ray source. The composition of the ash samples as measured from the WD-XRF is tabulated in Table 1. The major components of all of the ash samples were found to be SiO_2 , Fe_2O_3 , Al_2O_3 and CaO .

Table 1: Major chemical components of various ashes measured by WD-XRF in wt%

Component (wt %)	Lignite	Bituminous	PRB	JBPS
SiO_2	32.8	25.3	22.1	49.9
CaO	31.7	2.3	42.2	9.4
Al_2O_3	14.2	13.5	10.5	11.5
Fe_2O_3	9.8	52.7	6.1	14.5
MgO	3.6	0.6	6.9	1.7
TiO_2	2.6	1.9	2.2	3.0
SrO	1.3	0.1	0.3	0.7
SO_3	1.2	0.6	5.7	1.2
K_2O	1.0	2.0	0.5	1.6
Na_2O	0.8	0.3	1.8	3.7

The bituminous ash was found to have unusually high iron oxide content for a coal ash of this variety. Since iron can take multiple valences, the chemical effects on the melting and subsequent viscosity of this iron are complex. The other ash samples have significantly lower iron content. The CaO content in the PRB ash is also exceedingly high. CaO , which acts as a network modifier, is typically thought to reduce the viscosity of glass. However, if a large amount is present, this may not be enough network formers to form a long-range glassy structure.

To that end, the ratio of network modifiers such as CaO , MgO , Na_2O and K_2O to network forming species such as SiO_2 and TiO_2 is highly relevant. Iron oxide as well as aluminum oxide can take on the role of network former or modifier depending on the oxidation state and relative amount present. If these species are excluded from the ratio, the lignite, bituminous, PRB, and JBPS ashes have molar ratios of modifiers to formers of 1.2, 0.18, 2.4 and 0.33 respectively. With a ratio of 2.4, the PRB ash has a very high content of modifiers, which would lead to a lower viscosity. A ratio of 1.2 as seen in the lignite will result in a low viscosity glass at high temperatures compared to a ratio of 0.18 observed in the bituminous ash or the 0.33 in the JBPS ash. It has been found

that ash types with high content of modifiers are more likely to penetrate and cause spallation of Thermal Barrier Coatings (TBC). Though the vanes in this study were not coated with TBC this observation may give insight into the propensity of particles to stick onto vane surfaces based on their chemical makeup.

Before being used in these experiments, the bituminous and JBPS ash samples were mechanically ground and then a laser based Coulter Counter was used to determine the mean diameter. The size distribution for the bituminous and JBPS ash types are shown in Figure 4 with the mean diameters marked. The mean diameters of the lignite and PRB ash types are also noted on Figure 4, these ash samples had been previously processed in a cyclone separator and their mean diameters supplied by Southern Electric Co.. Nothing further was done to them before they were used in experiments

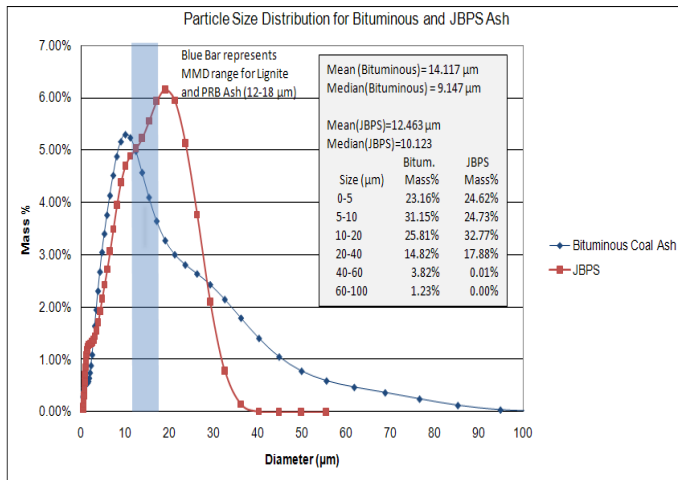


Figure 4: Particle size distribution for ground bituminous and JBPS coal fly ash with indications of MMD for other tested ash types.

EXPERIMENTAL DISCRIPTION

The operating conditions examined in the current study are shown below in Tables 2 and 3. Table 2 shows tests that did not involve film cooling, while Table 3 shows tests with film cooling. The Stokes number was calculated using the equation below with the leading edge diameter of the vane being used for the length scale. Since only a range of MMD was obtained for the lignite and PRB ash types a representative value of 15μm for particle diameter was used; the measured MMD's stated in Figure 4 were used for both the bituminous and JBPS ash types. Particle density was measured for all 4 ash types and inlet conditions were used as representative values for the flow variables.

$$St = \frac{\rho_p D_p^2 u_\infty}{18\mu L} \quad (1)$$

The facility was run once with each sub-bituminous ash type, and twice with bituminous and lignite. One of the tests with lignite and bituminous included film cooling and one did not. The film cooling massflow rate is indicated as a percent of vane inlet massflow. The film cooling was split evenly to the hub and casing side of the vanes.

Table 2: No Film Cooling Test Conditions

Ash Type Tested	Bituminous	JBPS	PRB	Lignite
Inlet Mass Flow	0.566	0.381	0.39	0.371
Inlet Temperature (°C)	1080	1044-1070	1042-1112	1041-1098
Inlet Mach Number	0.09	0.086	0.09	0.082
Exit Re	351900	237900	242000	23700
Test Time (hrs)	0.55	0.25	1.1	0.48
Particle Loading (ppmw)	1000	780	380	550
Particle Concentration (ppmw-hr)	244	93.5	86.1	87.6
Stokes Number	1.58	1.02	0.43	0.83

Table 3: Film Cooling Test Conditions

Ash Type Tested	Bituminous	Lignite
Inlet Mass Flow (kg/s)	0.557	0.371
Inlet Temperature (°C)	1037	1037
Inlet Mach Number	0.098	0.078
Exit Re	348,200	230,000
Test Time (hrs)	0.55	0.29
Particle Loading (ppmw)	519	680
Particle Concentration (ppmw-hr)	285	101
Film Cooling	11.60%	8.30%
Density ratio	1.83	1.86
Stokes Number	1.58	0.95

Test conditions were defined by the inlet gas temperature and inlet mass flow rate. In Table 2, where there is a range of inlet temperatures the test began at the lower value and was increased by 12° C every 10 minutes until the upper limit was reached. Inlet temperatures were held to ± 6° C from the value selected and mass flow rate was held to ± 0.01 kg/sec. All temperature measurements have an uncertainty of 2%. The choked flow orifice plate flowmeters have a 3-5% uncertainty for the massflow rates investigated. Uncertainties were calculated using the uncertainty analysis from Coleman and Steele [15].

This facility operates under the principle validated by Jensen et al. [12] that the fundamental mechanisms of deposition are dominated by net particulate throughput, while particle concentration and test time are not independently significant. This allows the TuRFR to operate at much higher particle concentrations for a shorter amount of time and produce deposits similar to those found on in-service power turbine hardware. For example, one hour at 1000 ppmw particle loading could simulate 1000 hours (1.5 months) of continuous operation at 1ppmw.

RESULTS

Effect of Coal Rank on Deposition without Film Cooling

The first battery of tests was aimed at determining if coal rank has an effect on the nature of deposition. As shown in Table 1 various coal ashes from different sources have different chemical structures. Video was taken of the vanes during the tests so that the growth of deposition could be monitored directly.

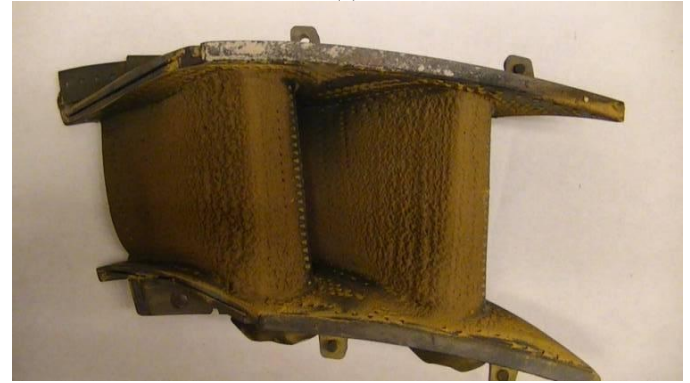
It was observed in these videos that the lignite coal ash deposited much more readily and at lower temperatures than the other ash types. When tests were begun at inlet temperatures of 1044 °C the lignite was observed to immediately begin to agglomerate on the vanes at an extremely high rate. When the sub-bituminous ash types were tested at the same inlet temperature, deposits did not grow very quickly. Only when the inlet temperature was increased to around 1050°C did deposits begin to agglomerate as quickly as was noted at lower temperatures with the lignite. The bituminous coal ash deposited the least and deposition did not begin to form until higher temperatures. At inlet temperatures of 1044°C the bituminous ash did not deposit at all; it was not until the temperature was increased to 1060°C that the bituminous began to deposit on the blades and only then at a very reduced rate. For these reasons it was concluded that lignite coal ash has a sticking temperature below 1044°C while sub-bituminous coal ash has a sticking temperature around 1050°C and bituminous coal ash has a sticking temperature above 1060°C. The higher growth rates of the lignite and sub-bituminous produced much thicker deposits than did the bituminous coal ash. Figure 5 shows a comparison of the same doublet after being exposed to each ash type.

From the video one could also observe the character of the deposition growth. For all ash types the first particles to stick impact the film cooling holes near 50% chord. Distributed buildup then begins to form farther back on the vane tending slightly towards the hub side. An image taken after the first 60 seconds of the JBPS, no film cooling test is shown in Figure 6. From this point deposits start to form on pre-existing deposits and fill in the spaces between film cooling holes. This process begins near the trailing edge and as time passes the deposits migrate toward the leading edge. The effect of deposits being more likely to deposit on pre-existing deposits was also noted by Crosby et. al and Kim et al. [13, 2]

Figure 7 is a video still taken 10 minutes after Figure 6 and at a higher inlet temperature, showing the growth of the deposits. The final picture taken after the vanes had been removed from the TuRFR is shown in Fig. 5(c).



(a)



(b)



(c)



(d)

Figure 5: Side by Side Comparison of (a) Bituminous, (b) PRB (c) JBPS and (d) Lignite coal ash deposits. Test conditions in Table 2.

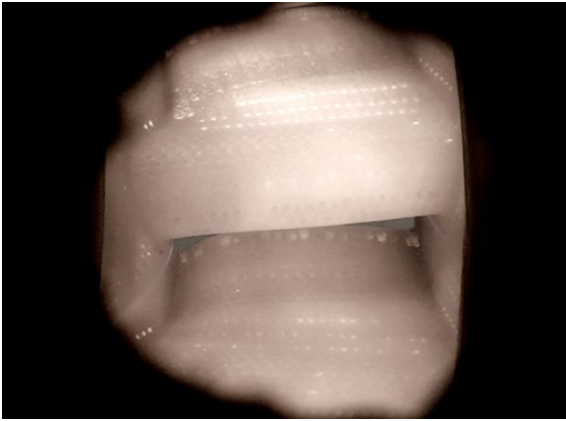


Figure 6: 60 Seconds into JBPS Sub-Bituminous Fly Ash Test- 1044°C see Table 2

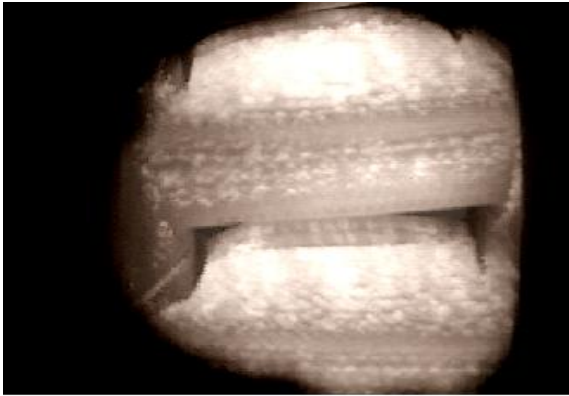


Figure 7: JBPS Fly ash ~1056°C, 11 minutes into test

Deposition Structure

After the tests were completed, the vanes were removed and their condition documented with photos and optical surface metrology.

Deposits were primarily on the pressure surface, coating the vane from leading to trailing edge. As mentioned before the deposits grow in the upstream direction. This feature is illustrated by the upstream-facing, jagged shape of the deposits [see Figs 5(c) & (d)] and likely occurs because of the propensity of deposits to stick to pre-existing deposits. The suction surface only had deposits on the initial 18% of the wetted distance of the vane. Common features of the pressure surface deposition structure are: a well defined stagnation line at the leading edge followed by lines of large jagged structures, and a very smooth deposit structure for the last 20% of the vane. These features are shown best in Figure 5d. It is likely that due to high shear stresses caused by increased local Mach number on the suction surface and near the trailing edge on the pressure surface that deposition formation is mitigated there. This phenomenon will be investigated further in Part II [9]. The bituminous coal ash did not deposit as readily as the other three ash types. It is likely that the lack of deposition is due to a higher sticking temperature with this ash.

Optical scans of the deposit structure were made after each test. This method has been demonstrated to detect deviation down to 0.1mm. A nominal model of the doublets had previously been created while the vanes were free of

deposits. A computer algorithm is used to compare the deposit model to the nominal model. In this way the deposit thickness can be examined without removing the very fragile deposits from the vanes. Figure 9 shows a scan of the vanes with JBPS ash deposits from Fig. 5(c). The red regions indicate deposits of 0.5 mm or greater in thickness.

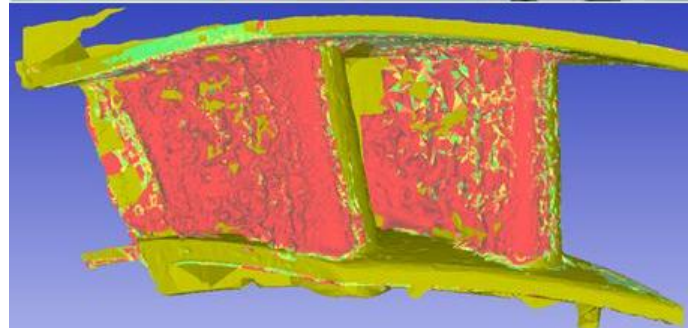
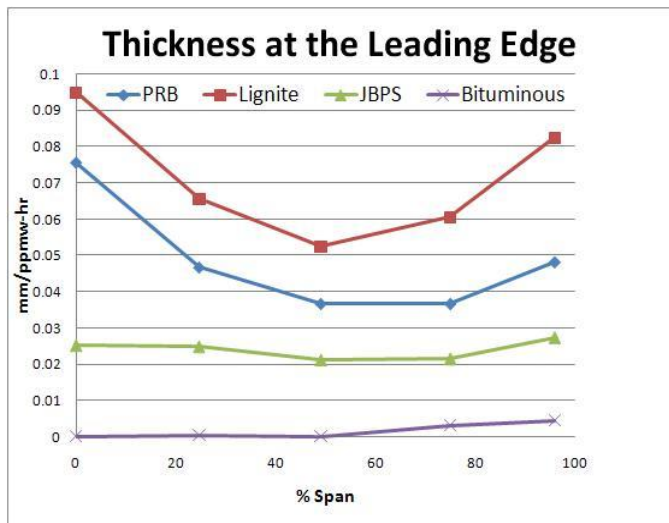


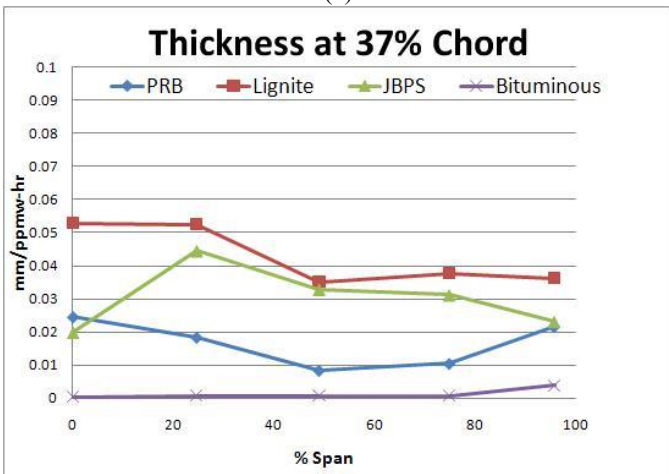
Figure 9: Surface metrology of vanes with JBPS ash deposit. Compare to Fig. 5(c).

These scans were interrogated at specific points to determine deposit thickness. A plot of thickness at various chord positions is shown in Figure 10a, b and c. The deposit thickness was measured in the surface normal direction. Subsequent measurements of deposit thickness in the axial direction (parallel to the inlet velocity) showed only minor changes from the trends shown in Fig. 10, indicating that the deposit locations are governed by more than just line of sight. This is consistent with the mean Stokes number of approximately unity (Tables 2 & 3). Deposit thickness is normalized by net particulate loading (ppmw-hrs) to remove the dependency thickness has on the total quantity of particulate injected into the gas stream during the test.

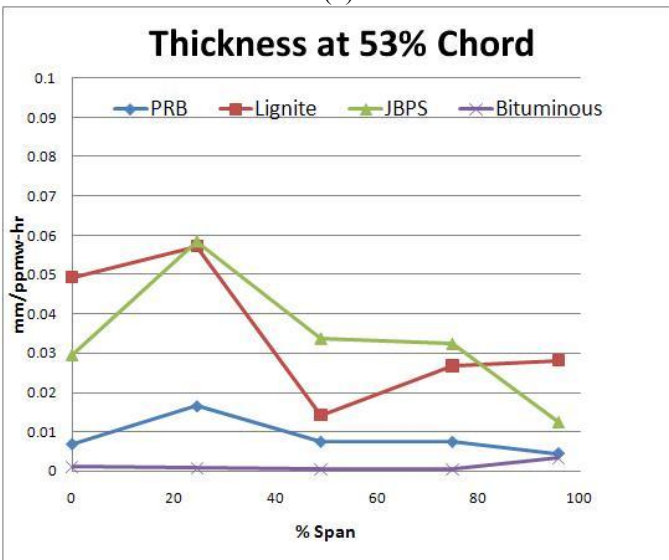
Figure 10a illustrates the increase in deposit thickness near the hub and casing end walls on the leading edge. Figures 10(b) and (c) (at 37 and 53% chord respectively) illustrate the tendency for deposits to stick near the hub side of the vane at mid chord positions. As was mentioned earlier, particles tend to stick to pre-existing deposits, and this gives rise to a non-linear deposit growth rate. Thus, the data in Figure 10 should not be used to predict deposition thickness for a set amount of time of turbine exposure to an arbitrary concentration of ash particulate. Deposition results documented from in service hardware compare well with the location and shape of the deposits for the current study. Kim et al. noted that the overwhelming majority of deposits were on the pressure surface near the leading edge [2]. Dunn et al. also noted that the heaviest deposits were located on the pressure surface and that deposits are extremely brittle [3]. Figure 11, taken from the RB211 that ingested volcanic ash from Mt Gallungung on 24 June 1982, shows these large scale deposits on the pressure surface of turbine NGV's with the thickest deposits near the leading edge and pressure surface [16].



(a)



(b)



(c)

Figure 10: Thickness comparison at (a) Leading Edge (b) 37% Chord (c) 53% Chord

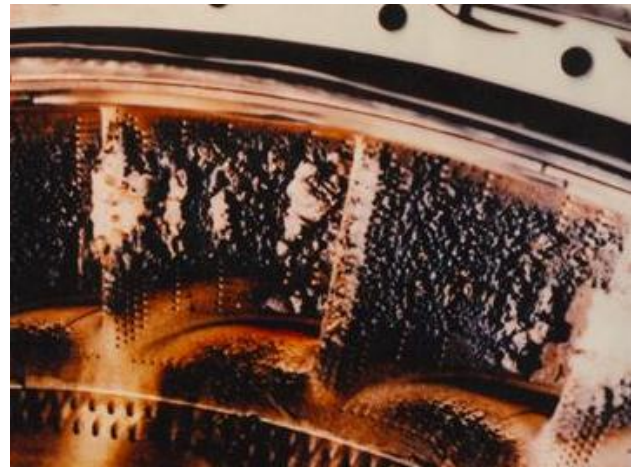


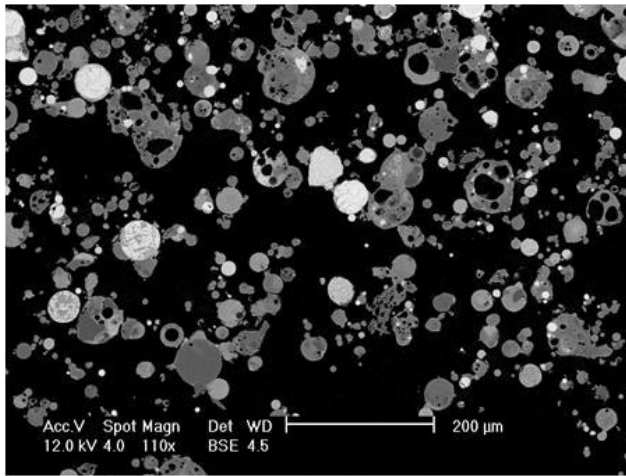
Figure 11: Volcanic Ash Deposits on pressure surface of NGV's (from Chambers [16])

Deposition Elemental Makeup

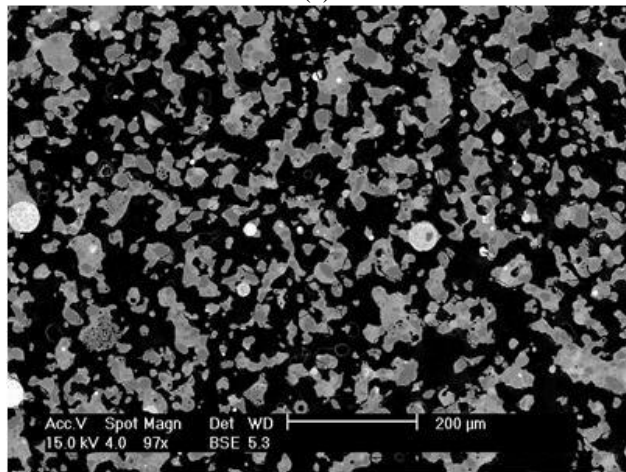
Deposits were removed from the turbine blades and mounted in epoxy. The mounted samples were sectioned and polished to one-micron surface finish using standard metallographic procedures. The polished samples were then examined by scanning electron microscope (SEM) equipped with an energy dispersive spectrometer detector (EDS).

Figure 12 shows two micrographs of deposits removed from the bituminous and JBPS ash tests; the black background in the SEM photos is the epoxy used to mount the deposit and maintain deposit stability during polishing. The deposits are all very porous, showing a planar view of the deposition particles within the large-scale structures. The bituminous deposit (Figure 12a) appeared to be the least dense, while the JBPS deposit (Figure 12b) and lignite deposits appear to have similar densities. Using these SEM images, the ratio of light regions (particulate) to dark regions (void) was used to determine the relative density of the ash particulate. The JBPS deposit was found to have 16% more total particulate in the image compared to the bituminous ash, confirming that it is more dense. Also of note, the JBPS deposit appears to have sintered to a greater extent than the other deposits. The mechanism of this sintering is currently under investigation.

Discrete sections of Si, Ca and Al rich particulates can be seen, indicating that the fusion of particles did not occur, nor phase separation occurred on cooling. An EDS micrograph of the JBPS deposits is shown in Figure 13. This figure shows that deposit structure consists almost entirely of Silicon and Calcium. As can be seen in Table 1 the lignite, JBPS and PRB ash samples have a high total weight percentage of SiO₂ and CaO (64.5%, 59.3% and 64.3% respectively) while the bituminous ash has a total weight percentage with these two elements of 27.6%. Since CaO reduces glass viscosity and the bituminous sample has a low ratio of modifiers to formers, this may explain the trend observed in Figure 10 with vastly thicker deposits being produced in the lignite and two sub-bituminous tests. The lack of fusion and phase separation was prevalent across the entire deposit, in a macro scale the deposits were uniform in thickness and there was no noticeable difference between deposits taken from the leading edge and trailing edge.



(a)



(b)

Figure 12: SEM photo of (a) bituminous ash deposit and (b) JBPS ash deposit (black background is epoxy filler, test conditions are presented in Table 2)

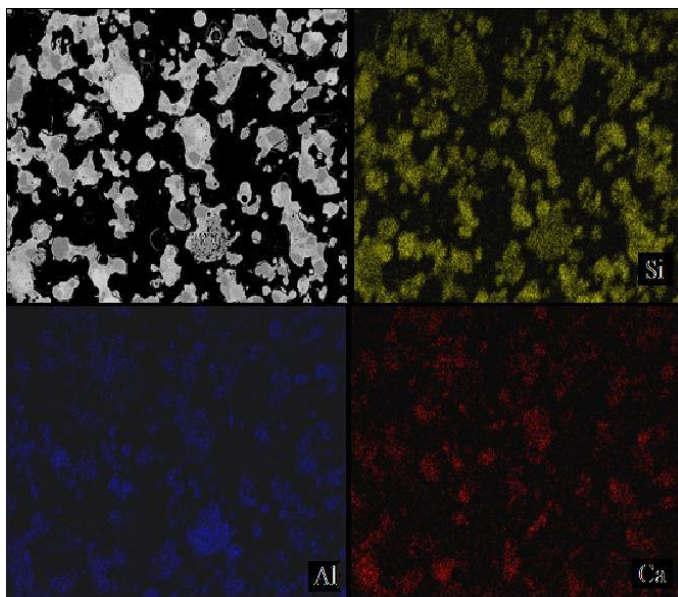


Figure 13: EDS micrographs of JBPS fly ash, showing concentrations of Si, Al, and Ca (350μm x 450 μm)

Effect of Film Cooling on Deposition

Film cooling effects were investigated for only two of the four ash types, bituminous and lignite fly ash. The test conditions are indicated in Table 3. In the bituminous film cooling test, it is interesting to note that the location of the deposits did not change from the non-film cooling case. The film cooling holes were still primary locations for deposit formation. For the test with film cooling, Figure 14a shows large scale deposits in film cooling holes near the leading edge. In the non film cooling case there was a thin coating of deposit, on the order of 0.1 mm thick, that covered the entire pressure surface (Figure 14b), in addition to large deposits at the film cooling holes. In the film cooling case there was no thin layer of deposit and bare metal was visible on the pressure surface (Figure 14a). Thus, for bituminous ash at these operating conditions, film cooling had a noticeable effect on deposition.

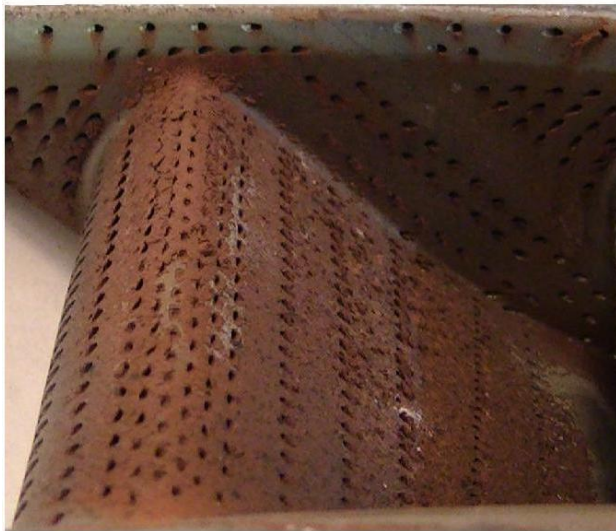
When comparing the lignite fly ash film cooling test to the non-film cooling test there was no significant difference in the final deposit structure. However it was noted from the video taken during the test that deposit formation was delayed several minutes. Once deposits did begin to form and film cooling holes became severely blocked the deposition rate of growth increased significantly and the deposits proceeded to grow in the same manner on the pressure surface as noted in the non film cooling case. It is interesting to note that there was a lack of deposition on the hub and casing end wall with film cooling. It is likely that these are the last film cooling holes to be blocked. With a large portion of the other film cooling holes blocked and the same amount of mass flow being applied to the film cooling cavities, the mass flow rate through these end wall film cooling holes was significantly increased.

Deposit Removal

Deposit removal both during and after a test is an effect that has been noted in the literature by various sources [2, 13, 14]. In the current study two mechanisms are thought to cause the deposit removal, aerodynamic drag and differential thermal coefficients of expansion. During test conditions deposit removal occurs due to the increase in drag that larger deposits experience as they protrude significantly into the flowfield. Video evidence was recorded of large particles sticking together in a small region and then being removed when the drag created by their size overcomes the sticking force. Removal of deposits was also observed during the cool down phase of operation. This occurs due to the difference in thermal expansion coefficient between the deposit and NGV, causing the brittle deposit to crack and fall off as the vanes cool and contract more rapidly. Once the deposit is shed, it leaves behind a residue that alters the original smooth surface of the vane.



(a)



(b)

Figure 14: Comparison of Bituminous Fly ash tests (a) Film Cooling (b) Non-Film Cooling

DISCUSSION

Dominant Factors of Deposition Growth

This study has verified that gas temperature has a first order effect on deposition growth in turbines. This conclusion agrees well with literature where an increase of deposit size and thickness with temperature is well documented. This study has also shown that not only is deposition governed by gas temperature but the chemical makeup of the ash also plays a crucial role in deposit formation. The four ash types studied here produced significantly different deposit thickness based on the rank of coal used to derive the ash.

Film Cooling Effect

Film cooling was observed to have a significant effect in the case of bituminous fly ash and almost no effect in the case of lignite fly ash. It is likely that the film cooling was more effective in the bituminous case because the film cooling jets were able to lower the vane temperature to a point significantly less than the melting temperature of the

bituminous fly ash and therefore mitigate the growth of deposits. During the lignite test the film cooling air was not cool enough to lower the vane surface to a temperature less than the melting temperature of the lignite fly ash and therefore only delayed the growth of deposits. The growth of deposits inside film cooling holes in both cases, even with blowing, suggests that surface impurities may also be a primary factor to consider when trying to mitigate deposition.

Operational Considerations to Avoid Deposits

The removal of deposits while the facility is running bodes well for continued operation even though a significant amount of particulate may have been ingested into the engine. The sloughing off of deposition during cool down suggests that reducing turbine inlet temperature may cause large deposits to fall off. These factors will most likely only delay problems to turbine components but not eliminate completely the harmful effect of deposition. In operation it would be best to avoid deposition by using the most effective air and fuel filtering systems feasible and keeping these systems in pristine condition. Also, by using coal of higher rank, higher vane inlet temperatures can be reached before deposit formation is inevitable.

CONCLUSIONS

Coal rank and consequently elemental composition was determined to have a profound effect on the size of deposits. Thickness measurements were taken using CMM scans for bituminous, lignite, and two sub-bituminous coal ash types. It was found that the overall thickness of lignite deposits was greater than that of the two sub-bituminous ashes. Observations from various literary sources were confirmed by the result that vanes become better captors of particulate as deposits grow larger, in other words particulate is more likely to deposit upon pre-existing deposition. Film cooling was found to have a minimal effect on the rate of deposition growth for the lignite ash type but a significant effect in the case of bituminous coal ash. While large deposit growth was only delayed when using lignite fly ash in film cooling cases, deposit growth and surface roughness were shown to be decreased in the case of bituminous fly ash with film cooling. SEM interrogation showed that deposits were very porous consisting of discrete sections of Si, Mg, and Al rich particles, this in-homogeneity was uniform throughout the deposit.

ACKNOWLEDGEMENTS

Special thanks to George Sandusky at GE and Dr. Mike Benzakein at OSU for helping to obtain the vane doublets and to Carl Landham at Southern Company for ash samples. Thanks to Rick Hayek from AEP Ohio for providing the bituminous coal ash. Thanks also to John McDaniel at Polk Power Station for helpful discussion. The authors would particularly like to recognize the assistance of Dr. Thomas Fletcher at BYU as well as Nathan Frost at Nikon Metrology for his work with the CMM machine and scanning the vanes. Also, thanks to Dr. Mike Dunn for his time and wisdom. We are indebted as well to Carey Clum for his hours of hard work keeping the facility running and Chris Smith for his patience in illustrating how to operate the facility. This work was

sponsored by a grant from the US Department of Energy and The Ohio State University Department of Mechanical and Aerospace Engineering. The views expressed in the article are those of the authors and do not reflect the official policy or position of the Department of Energy or U.S. Government.

NOMENCLATURE

ppmw-hr	Parts per million by weight hour
Re	Reynolds number based on NGV chord
St	Stokes number based on NGV leading edge diameter, Eq. (1)
ρ_p	Particle Density
μ	Fluid Viscosity
u_∞	Vane Inlet Velocity
D_p	Particle Diameter
L	Vane leading edge diameter

REFERENCES

- [1] Wenglarz, R.A., Fox, R.G. Jr. "Physical Aspects of Deposition from Coal-Water Fuels Under Gas Turbine Conditions", J. Engr. Gas Turbine & Power. Vol 120, Jan 1990, pp9-14.
- [2] Kim, J., Dunn, M.G., and Baran, A.J. et al, "Deposition of Volcanic Materials in the Hot Sections of Two Gas Turbine Engines," J. Engr. Gas Turbines & Power. Vol 115, Jul 1993, pp 641-651.
- [3] Dunn, M G., Baran, A. J., Miatech, J. "Operation of Gas Turbine Engines in Volcanic Ash Clouds" J. Engr. Gas Turbines & Power. Vol 118, Oct 1996, pp 724-731.
- [4] Wenglarz, R.A., "An Approach for Evaluation of Gas Turbine Deposition," J. Engr. Gas Turbines & Power. Vol. 114, April 1992, pp 230-234
- [5] Bogard, D.G., Schmidt, D.L., Tabbita, M., "Characterization and Laboratory Simulation of Turbine Airfoil Surface Roughness and Associated Heat Transfer," J. Turbomachinery. Vol 120, April 1998, pp 337-342.
- [6] Hussein, M. F., and Tabakoff, W., "Computation and Plotting of Solid Particle Flow in Rotating Cascades," *Computers and Fluids*, Vol. 2, No.1, 1971, pp.1-15
- [7] Tabakoff, W., and Hussein, M.F., "Trajectories of Particles Suspended in Flows Through Cascades," *Journal of Aircraft* Vol. 8, No.1, 1971, pp.60-64
- [8] Tafti, Danesh K., and Sreedharan, S.S., "Composition Dependent Model for the Prediction of Syngas Ash Deposition with the Application to a Leading Edge Turbine Vane." *ASME Turbo Expo 2010: Power for Land, Sea, and Air* (2010).
- [9] Barker, B., Casaday, B., Shankara, P., Ameri, A., Bons, J.P. "Coal Ash Deposition on Nozzle Guide Vanes: Part II-Computational Modeling," Accepted for publication to ASME Turbo Expo 2011: Power for Land, Sea, and Air. June 14-18, 2011, Vancouver, Canada. Paper # GT2011-46660
- [10] Lawson, S.A., Thole, K., "The Effects of Simulated Particle Deposition on Film Cooling," presented at ASME Turbo Expo: Power for Land, Sea, and Air. June 8-12, 2009, Orlando, Florida USA. Paper #: GT2009-59109.
- [11] Vandsburger, U., Tafti, D, Ng, W., "Syngas Particulate Deposition and Erosion at the Leading Edge of a Turbine Blade with Film Cooling." Presented at UTSR Workshop, Oct 27-29, 2009, Orlando, FL, USA.
- [12] Jensen, J.W., Squire, S.W., Bons, J.P., Fletcher, T.H., "Simulated Land-Based Turbine Deposits Generated in an Accelerated Deposition Facility," J. Turbomachinery. Vol. 127, July 2005, pp 462-470.
- [13] Crosby, J.M., Lewis, S., Bons, J.P, Ai, W., Fletcher, T.H., "Effects of Particle Size, Gas Temperature, and Metal Temperature on high Pressure Turbine Deposition in Land Based Gas Turbines from Various Synfuels," presented at ASME Turbo Expo 2007: Power for Land, Sea, and Air. May 14-17, 2007, Montreal, Canada. Paper #: GT2007-25731.
- [14] Smith, C., Barker, B., Clum, C., Bons, J., "Deposition in a Turbine Cascade with Combusting Flow." Presented at ASME Turbo Expo 2010: Power for Land, Sea, and Air. June 2010, Glasgow, Scotland. Paper #:GT2010-22855
- [15] Coleman, H.W., Steele, W. G. Experimentation and Uncertainty Analysis for Engineers. 2nd Edition. Wiley Interscience. 1999.
- [16] Chambers, J.G., "The Volcanic Cloud Encounter of a Rolls-Royce Powered Boeing 747 of the British Airways Fleet 24 June 1982," Internal Rolls-Royce Report, January 1985.